

FXR agonist GW4064 enhances anti-PD-L1 immunotherapy in colorectal cancer

Lu Lu^{a,b##}, Yi-Xin Jiang^{a##}, Xiao-Xia Liu^{a##}, Jin-Mei Jin^{a##}, Wen-Jie Gu^a, Xin Luan^a, Ying-Yun Guan^c, and Li-Jun Zhang^a

^aShanghai Frontiers Science Center of TCM Chemical Biology, Institute of Interdisciplinary Integrative Medicine Research, Shanghai University of Traditional Chinese Medicine, Shanghai, China; ^bCenter for Clinical Pharmacy, Cancer Center, Department of Pharmacy, Zhejiang Provincial People's Hospital (Affiliated People's Hospital, Hangzhou Medical College), Hangzhou, China; ^cDepartment of Pharmacy, Ruijin Hospital, Shanghai Jiaotong University School of Medicine, Shanghai, China

ABSTRACT

Colorectal cancer (CRC) is one of the top three malignant tumors in terms of morbidity, and the limited efficacy of existing therapies urges the discovery of potential treatment strategies. Immunotherapy gradually becomes a promising cancer treatment method in recent decades; however, less than 10% of CRC patients could really benefit from immunotherapy. It is pressing to explore the potential combination therapy to improve the immunotherapy efficacy in CRC patients. It is reported that Farnesoid X receptor (FXR) is deficiency in CRC and associated with immunity. Herein, we found that GW4064, a FXR agonist, could induce apoptosis, block cell cycle, and mediate immunogenic cell death (ICD) of CRC cells *in vitro*. Disappointingly, GW4064 could not suppress the growth of CRC tumors *in vivo*. Further studies revealed that GW4064 upregulated PD-L1 expression in CRC cells via activating FXR and MAPK signaling pathways. Gratifyingly, the combination of PD-L1 antibody with GW4064 exhibited excellent anti-tumor effects in CT26 xenograft models and increased CD8⁺ T cells infiltration, with 33% tumor bearing mice cured. This paper illustrates the potential mechanisms of GW4064 to upregulate PD-L1 expression in CRC cells and provides important data to support the combination therapy of PD-L1 immune checkpoint blockade with FXR agonist for CRC patients.

ARTICLE HISTORY

Received 4 February 2023
Revised 18 May 2023
Accepted 18 May 2023

KEYWORDS

Colorectal cancer; farnesoid X receptor; GW4064; PD-L1

Introduction

Colorectal cancer (CRC) has high morbidity and mortality worldwide, with more than 1.85 million newly confirmed cases and 0.85 million deaths each year¹. Genetic inheritance, poor dietary habits, and lifestyle factors can affect the development of CRC². At present, surgery is still the preferred treatment option, and the combination of chemical, radiological, and targeted therapy has significantly prolonged the survival time of CRC patients. However, the clinical treatment and diagnosis of metastatic CRC is still a problem, and the patients' five-year survival rate with metastatic CRC is less than 20%³.


Unlike traditional chemotherapy drugs, immunotherapy is a novel therapeutic strategy for cancer treatment, aiming to exert a highly effective tumor killing effect by reactivating or enhancing the body's anti-tumor immune response⁴. Programmed death-ligand 1 (PD-L1) is the most used drugs targeting immune checkpoint molecules, whose binding with its receptor (PD-1) results in suppressing the anti-tumor immunity⁵. Blocking the interaction between PD-L1 and PD-1 has become a promising treatment for cancer⁶. PD-L1/PD-1 antibodies, such as Atezolizumab, Nivolumab, and Avelumab, et al., have witnessed the success and encouraging efficacy in multiple human cancers, including non-small cell lung cancer (NSCLC), advanced melanoma, and bladder cancer⁷. However,

less than 10% of CRC patients could really benefit from immunotherapy⁸. Thus, the new combination therapy strategies are critical to enhance the efficacy of immunotherapy for CRC patients.

Farnesoid X receptor (FXR, NR1H4), functioning as an important regulator of bile acids homeostasis, could regulate the transcription of numerous genes including lipid, glucose, and amino acid metabolism in the gut–liver axis^{9–12}. Recent studies have found that FXR is deficiency in CRC, hepatocarcinoma carcinoma (HCC), and cholangiocarcinoma (CCA)^{13–15}, but overexpression in NSCLC, pancreatic cancer, and thyroid cancer^{16–18}. The abnormal expression of FXR is associated with the disorder of bile acids, destruction of intestinal flora, secretion of inflammatory cytokines, and poor prognosis of tumor patients, revealing that FXR is involved in the regulation of inflammation, immunity, and tumorigenesis^{19–21}. Evidences suggest that PD-L1 low/negative NSCLC patients receiving anti-PD-1 immunotherapy have favorable clinical outcomes when their FXR expression is high²². And in mice, the PD-1 antibody is effective against FXR^{high}PD-L1^{low} Lewis lung carcinoma (LLC), indicating that FXR regulation might be an effective strategy to combat cancers combined with immunotherapy²³. It is demonstrated that there is a negative correlation between tumor stage and prognosis and the

CONTACT Xin Luan  luanxin@shutcm.edu.cn; Li-Jun Zhang  zhanglijun0407@shutcm.edu.cn  Shanghai Frontiers Science Center of TCM Chemical Biology, Institute of Interdisciplinary Integrative Medicine Research, Shanghai University of Traditional Chinese Medicine, Shanghai 201203, China; Ying-Yun Guan  gyy40696@rjh.com.cn  Department of Pharmacy, Ruijin Hospital, Shanghai Jiaotong University School of Medicine, Shanghai 200025, China

[#]These authors are contributed equally to this work.

 Supplemental data for this article can be accessed online at <https://doi.org/10.1080/2162402X.2023.2217024>.

© 2023 The Author(s). Published with license by Taylor & Francis Group, LLC.

This is an Open Access article distributed under the terms of the Creative Commons Attribution-NonCommercial License (<http://creativecommons.org/licenses/by-nc/4.0/>), which permits unrestricted non-commercial use, distribution, and reproduction in any medium, provided the original work is properly cited. The terms on which this article has been published allow the posting of the Accepted Manuscript in a repository by the author(s) or with their consent.

downregulation of FXR in CRC tissues^{15,24–26}. Activation of FXR has a significant inhibiting effect on CRC progression^{27,28}. Hence, restoring the function of FXR might be a promising therapeutic strategy in combination with immunotherapy for CRC therapy.

GW4064, a FXR agonist, showed promising anti-tumor effects in multiple tumors, including breast cancer, liver cancer, and CRC^{29–32}. In present study, we found that GW4064 could inhibit the proliferation of CRC cells *in vitro* but not suppress the growth of CRC tumors *in vivo*. Further studies revealed that GW4064 upregulated PD-L1 expression in CRC cells via activating FXR and MAPK signaling pathways. And the combination of PD-L1 antibody with GW4064 exhibited excellent anti-tumor effects in CT26 xenograft models and increased CD8⁺ T cells infiltration, with 33% tumor bearing mice cured. This paper illustrates the potential mechanisms of GW4064 to upregulate PD-L1 expression in CRC cells and provides important data to support the combination therapy of PD-L1 immune checkpoint blockade with FXR agonist for CRC patients.

Materials and methods

Regent and cell lines

GW4064 was purchased from MCE (Shanghai, China). CRC cell lines HCT116 (human) and CT26 (mouse) were purchased from the National Collection of Authenticated Cell Cultures (Shanghai, China). The HCT116 cells and CT26 cells were cultured in a cell incubator with the appointed medium.

Cell viability assay

HCT116 and CT26 cells were seeded into 96-well plates (5×10^3 cells/well) overnight, and incubated with GW4064 at different concentrations for 24 h. Then the cells were incubated with fresh free-serum medium containing 10% Cell Counting Kit-8 (CCK-8, Beyotime, China) solution for another 2 h. Finally, the absorbance was measured using a Cytation 5 system (BioTek, USA) under 450 nm.

Live/Dead cell viability/cytotoxicity

HCT116 and CT26 cells (1×10^4 cells/well) were seeded into 96-well plates overnight and treated with GW4064 for 24 h. Then the fresh medium containing calcein-AM (2 μ M) and propidium iodide (PI, 8 μ M) was added to incubate for 15 min. The cells were observed and photographed by a high content analysis imaging system (PE, USA).

Real-time cell growth inhibition

5×10^3 cells each well of HCT116 and CT26 cells were seeded into E-Plate overnight and treated with or without GW4064 at various concentrations for 24 h. Real-time cell proliferation and cytotoxicity were measured by a xCELLigence RTCA system (Agilent, USA).

Apoptosis assay

To explore apoptosis *in vitro*, HCT116 and CT26 cells (3×10^5 cells/well) were seeded in 6 well plates and treated with GW4064 for 24 h. Then the cells were collected and incubated with annexin V-FITC and PI for 10 min in the dark before being analyzed by flow cytometry.

Cell cycle arrest

HCT116 and CT26 cells treating with or without GW4064 were harvested and fixed in 75% ethanol overnight at -20°C . Then the fixed cells were washed twice with PBS and incubated with PI (BD Pharmingen, USA) for 15 min before analyzing by flow cytometry (CytExpert 3.0 software).

siRNA transfection

The FXR siRNA and NC were commercially obtained from GenePharma Biotech Company (Shanghai, China). The sequence of FXR siRNA1 was 5'-GCAACUGUGUGAUGGAUAUTT-3' and the sequence of FXR siRNA2 was 5'-GGAGAGUAAACGACCACAATT-3'. The negative control (NC) sequence was 5'-UUCUCCGAACGUGUCACGUTT-3'. According to the manufacturer's protocols, the cells were harvested for western blot assay after transfection for 48 h.

Proteomics

HCT116 cells were treated with 6 μ M GW4064 for 48 h, then extracted from the cell lysate. The samples were preliminarily treated using FASP enzymatic hydrolysis method³³. Finally, we use TMT to label the samples. The liquid phase was used for classification, and the final samples were detected by mass spectrometry. The results were analyzed using bioinformatics databases.

Western blot assay

The proteins of HCT116 and CT26 cells treating with GW4064 were collected, separated by 12% SDS-PAGE, and transferred onto polyvinylidene difluoride (PVDF) membranes. Then the PVDF membranes were blocked in 5% nonfat milk for 1 h and incubated with primary antibodies at 4°C overnight. After being incubated with secondary antibodies for another 1 h, the proteins were detected by Gel Imaging System (Tanon, China) and analyzed by Image J software.

Quantitative real-time PCR (Qrt-PCR)

PD-L1 mRNA expression was detected using qRT-PCR method. The total RNA was extracted from CT26 and HCT116 cells as well as CT26 xenograft tumors administered with GW4064. RNA was reverse transcribed into cDNA using the Reverse Transcription Kit HiScript[®] II Q RT SuperMix (Vazyme, R223-01). PCR reaction mixes were prepared according to the manufacturer's instructions for the ChamQ Universal SYBR qPCR Master Mix kit (Vazyme, Q711-02). The sequence of human PD-L1 gene:

forward 5'- GACCACCACCACCAATTCCAAGAG-3' and reverse 5'-TGAATGTGTCAGTGCTACACCAAGGC-3'. The sequence of mouse PD-L1 gene: forward 5'-GATTCAGTTTGTGGCAGGAGAGGAG-3' and reverse 5'-GGCATTGACTTTCAGCGTGATTCG-3'. The human primer GAPDH (Sangon Biotech, B661104) and the mouse primer GAPDH (Sangon Biotech, B661304) were used as internal control. Subsequently, PD-L1 mRNA expression was quantified using the Real-Time PCR System (Applied Biosystems).

HMGB1 and calreticulin (CRT) immunofluorescence staining

The HCT116 and CT26 cells treated with GW4064 were fixed and permeabilized with 4% paraformaldehyde for 20 min and 1% Triton X-100 for 5 min, respectively. Then incubated with the primary antibody of HMGB1 (Abcam, ab227168) at 4°C overnight, following incubating with secondary antibody conjugated with Alexa Fluor 488 for another 2 h. For CRT, the cells were stained with Alexa Fluor 488-CRT (Abcam, ab196159) for 1 h. Finally, stained the cell nucleus with Hoechst 33,342 and detected by GE DeltaVision OMX SR.

ATP release assay

HCT116 and CT26 cells (5×10^3 cells/well) were seeded in 96-well plates and treated with GW4064 at different concentrations for 6 h. Based on the protocols of ATP assay kit (Beyotime, S0027), the cell supernatant was analyzed by a luminometer (Tecan Spark, Switzerland).

Anti-tumor therapy

Female BALB/c mice (4–5 weeks) were obtained from Shanghai Sippr BK Laboratory Animals Ltd under SPF condition. These animal experiments obtained the ethics committee approve of Shanghai University of Traditional Chinese Medicine (No. PZSHUTCM220627046). 5×10^5 CT26 cells were subcutaneously inoculated into these mice on the right side of their armpits. The tumor volume was monitored every 2 days and calculated by the following formula: volume = (length \times width²)/2. Twelve mice were randomly divided into Control group and GW4064 (30 mg/kg, i.p.) group when the tumor volume was approximately 50 mm³. After treating with GW4064 for the appointed time, tumor tissues were collected for further studies.

Combination therapy

In female BALB/c mice, 5×10^5 CT26 cells were subcutaneously injected into the right armpit. When the average tumor volume reached about 50 mm³, the mice were randomly divided into four groups ($n = 6$): Control, GW4064 (30 mg/kg, i.p.), PD-L1 antibody (100 μ g per mouse, i.p.), and GW4064 + anti-PD-L1. Finally, the tumors were collected for further studies, including Elisa assay (IL-2, IFN- γ , and TNF- α), and histochemical analysis (H&E, Ki-67, TUNEL, CD4, and CD8).

Hematoxylin and eosin (H&E) stains

Tumor tissues were sectioned and fixed overnight in 4% paraformaldehyde (Servicebio, G1101), paraffin embedded and cut into 5- μ m-thick sections. Then the sections were stained with hematoxylin (Servicebio, G1004) for 5 min and then stained with eosin (Servicebio, G1001) after dehydration. After sealing, they were photographed under the microscope for analysis.

Immunohistochemistry (IHC)

Tumor tissue sections were deparaffinized with xylene and rehydrated in anhydrous alcohol solution. For IHC, the sections were incubated with 3% BSA blocking solution for 30 min, followed by incubation with primary antibodies of Ki67 (Servicebio, GB111499). Subsequently, the sections were incubated for 1 h with the secondary antibody conjugated with HRP. After the development reaction with DAB, the slices were photographed with the Cytation 5 system (BioTek, USA).

TUNEL assay

Tumor tissue sections were deparaffinized and hydrated with anhydrous alcohol solution for 3 min. Then, they were incubated with proteinase K (20 μ g/mL) and permeabilized with 0.1% Triton X-100 for 8 min. The kit (#11684817910, Roche) was further used to perform the TUNEL assay.

Flow cytometry detection of PD-L1 expression

To detect the expression of cell surface PD-L1, HCT116 and CT26 cells (3×10^5 cells/well) were seeded into 6 well plates and treated with GW4064 for 24 h. Then the cells were collected and stained with PE-conjugated anti-human-PD-L1 (Proteintech, 65073) and PE-conjugated anti-mouse-PD-L1 (BD Pharmingen, 561787) antibody for 30–40 min in the dark before being analyzed by flow cytometry.

Detection of immune-related cells

Single-cell suspensions of CT26 xenograft tumor tissues were prepared by tissue dissociation solution digestion, and then the 1×10^6 cells were resuspended with 100 μ L flow-staining buffer. Appropriate amounts of F4/80 (BD Pharmingen, 565411), CD11b (BD Pharmingen, 561691), CD86 (BD Pharmingen, 555665), CD45 (BD Pharmingen, 561586), CD3 (BD Pharmingen, 553240), CD4 (BD Pharmingen, 1116730), CD8 (BioGems Internation, 10122-80-100), CD25 (BD Pharmingen, 557192), and Foxp3 (BD Pharmingen, 560408) antibodies were added and incubated for 30 min at 4°C on ice in the dark before analyzed by flow cytometry. Among them, Foxp3 needs to be fixed and broken by 1% paraformaldehyde before staining.

Statistical analysis

All the data were analyzed using the GraphPad Prism 8.0.1 software, and the mean \pm standard deviation (SD) was calculated for at least three independent experiments. For

comparison between two groups or among multiple groups, an independent Student's t-test or two-way ANOVA followed by Tukey's test was used. * $P < 0.05$, ** $P < 0.01$, *** $P < 0.001$.

Results

GW4064 induced apoptosis and blocked cell cycle G2 transition of CRC cells

GW4064 is a FXR agonist with EC_{50} of 65 nM, and the chemical structure formula is shown in Figure 1A. Current studies have found that as a tool drug, GW4064 exhibits anti-tumor activities *in vitro*³². Herein, GW4064 could inhibit CRC cells (HCT116 and CT26) in a dose-dependent manner, and the IC_{50} of HCT116 and CT26 cells were 6.9 μ M and 6.4 μ M, respectively (Figure 1C). Using High Content Analysis System, we detected that GW4064 could inhibit half CRC cells at 6 μ M, as observed with CCK-8 assay (Figure 1B).

To monitor cell growth status in real time after drug treatment, quantitative cytotoxicity data were obtained using the RTCA xCELLigence system, which collected the data every 15 min to record tumor cell dynamics curves. Figure 1D,E showed that GW4064 could significantly inhibit the cell proliferation of HCT116 and CT26 cells within 12 h. And the results of flow cytometry showed that GW4064 could induce apoptosis (Figure 1F) and block the G2 phase of cell cycle (Figure 1G–I). The above experimental results showed that GW4064 did have anti-tumor effect *in vitro*.

GW4064 induced immunogenic cell death mediated by endoplasmic reticulum stress

It has been reported that farnesol, the earliest natural agonist of FXR, can increase endoplasmic reticulum (ER) stress-related protein expression (such as ATF3, CHOP, and XBP1) by MEK1/2 signaling pathway, which activated unfolded proteins to induce apoptosis of human lung cancer cell H460^{34–36}. In Figure 2A–C, GW4064 upregulated the phosphorylation of PERK/eIF2 α and increased ATF6 protein expression in HCT116 and CT26 cells, indicating that GW4064 could activate ER stress in CRC cells. Consistent with previous report, activating ER stress can promote immunogenic cell death (ICD)³⁷. It could be clearly seen that the ICD makers (CRT, HMGB1, and ATP) were significantly increased. The HMGB1 labeled green fluorescence in the cell nucleus was wakened after treated with GW4064 via immunofluorescence confocal experiment, while the expression of CRT labeled red fluorescence increased and was turned outward into the cell membrane (Figure 2D,E), and the secretion of ATP were dose-dependent increased (Fig. S1). These results indicated that GW4064 could induce ICD of CRC cells, triggering HMGB1 excretion, CRT exposure, and ATP secretion.

GW4064 did not suppress the growth of CT26 xenograft tumors *in vivo*

Since GW4064 could inhibit the proliferation of CRC cells effectively *in vitro*, the CT26 tumor-bearing BALB/c mice model was used to evaluate its efficacy (Figure 3A). When the

average tumor volume reached 50 mm³, a daily dose of GW4064 (30 mg/kg) was administered intraperitoneally, and there was no significant weight loss or abnormal behavior in each group of mice during administration (Figure 3C). The disappointing results showed that GW4064 could not suppress the growth of CT26 xenograft tumors *in vivo* (Figures 3B, 3D–E). And the poor therapeutic effect of GW4064 *in vivo* is further confirmed by H&E staining (Figure 3F,G). Surprisingly, the immunohistochemical assay showed that the PD-L1 was upregulated in the groups treating with GW4064 (Figure 3F,G), which might be the reason of the poor anti-tumor activity of GW4064. In addition, the protein expression and mRNA level of PD-L1 in tumor tissues were also increased (Fig. S2).

GW4064 upregulated PD-L1 expression in CRC cells by activating MAPK signaling pathway

Consistent with the previous results in Figure 3F,G, protein expression of PD-L1 was upregulated after treating with GW4064 in HCT116 and CT-26 cells, respectively (Figure 4A–C). Flow cytometry and qRT-PCR methods were further used to detect the cell surface and mRNA expression of PD-L1. The results showed that GW4064 induced the upregulation of cell surface and mRNA expression of PD-L1 (Fig. S3–S4). Then, a proteomic analysis of HCT116 cell treated with GW4064 was performed to explore the mechanisms involved in the upregulation of PD-L1. The results showed that multiple proteins involved in the MAPK signaling pathway were upregulated after being treated with GW4064 (Figure 4D, S5), and the raw data of proteomic analysis were displayed in Table S1. The expression of FGF-19/15 in HCT116 and CT26 cells was increased after GW4064 treatment via western blot assay, and the phosphorylation of JNK and ERK1/2 could be upregulated (Figure 4A–C). In HCT116 cells, when FXR was knocked down, the expression of PD-L1 also decreased (Figure 4E,F). And repression of FXR by siRNA and the inhibitor of MAPK signal pathway (VX-702) significantly reversed the upregulation effect of GW4064 on PD-L1 expression in HCT116 cells (Figures 4G–I, S6). These results suggested that GW4064 acted as a FXR agonist that activated the MAPK signaling pathway to modulate PD-L1 of CRC cells.

GW4064 enhanced the anti-PD-L1 immunotherapy in CT26 tumor-bearing mice

Considering that GW4064 could increase PD-L1 expression in tumor cells, we conducted combination therapy of anti-PD-L1 and GW4064 for CT26 tumor-bearing mice, which might improve the anti-tumor efficacy of GW4064 on immune-sound tumor-bearing mice. CT26 tumor-bearing mice treated with GW4064 were injected intraperitoneally with PD-L1 antibody on day 3, day 6, and day 9 during administration (Figure 5A). The results showed that although PD-L1 antibody had a certain inhibiting effect, tumor growth was significantly inhibited in the combination therapy (GW4064 + anti-PD-L1) group compared with control, and two of the six mice showed complete eradication of tumors (Figures 5B, 5D–F). Besides, no significant mouse body

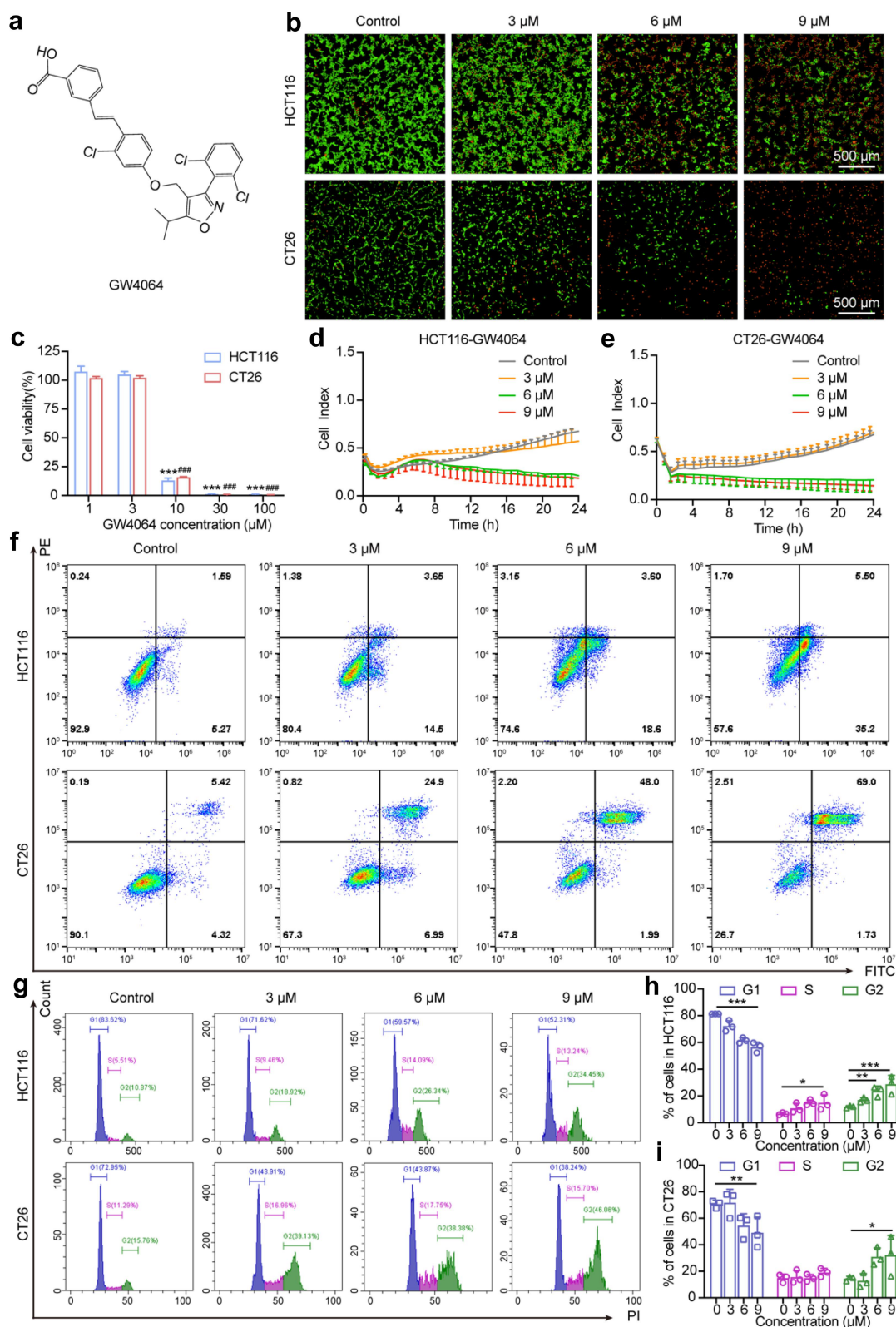


Figure 1. GW4064 inhibited CRC cells proliferation and induced apoptosis in vitro. (a) Chemical structure of GW4064. (b) HCT116 and CT26 cells proliferation was examined using CCK-8 assay after treatment with G4064 for 24 h. (c) HCT116 and CT26 cells after treatment with GW4064 were stained with LIVE/DEAD cell viability/cytotoxicity kit. Kinetic curves of the cytotoxicity of HCT116 (d) and CT26 (e) cells after treatment with GW4064 in different concentrations, as assessed by xCelligence RTCA. Flow cytometry detected apoptosis (f) and cell cycle arrest (g) of HCT116 and CT26 cells after treatment with GW4064. The HCT116 (h) and CT26 (i) cells were arrested in G2 phase. Data was presented as mean \pm S.D.; $n = 3$. Statistical significance: * $p < 0.05$, ** $p < 0.01$, *** and ### $p < 0.001$.

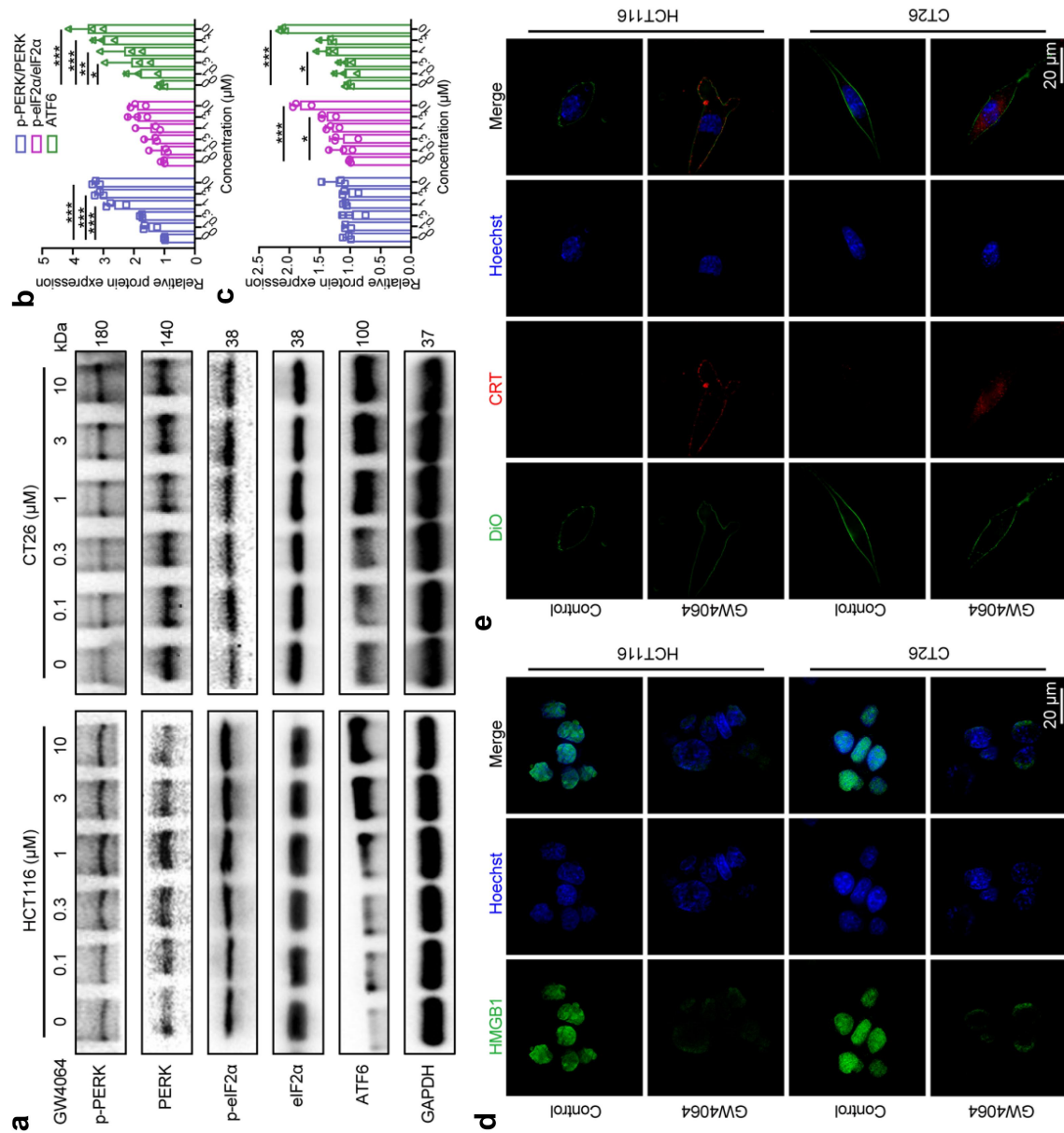


Figure 2. GW4064 induced ICD mediated by ER stress. (a) GW4064 treatment for 48 h increased the phosphorylated protein expression of PERK and eIF2α, and upregulated the protein expression of ATF6 in HCT116 and CT26 cells. Statistical assay of the relative protein contents in HCT116 (b) and CT26 (c) cells. (d) GW4064 promoted HMGB1 protein excretion (d) and CRT protein excretion (e) in HCT116 and CT26 cells by immunofluorescence confocal experiments. Data was presented as mean \pm S.D.; $n = 3$. Statistical significance: * $p < 0.05$, ** $p < 0.01$, *** $p < 0.001$.

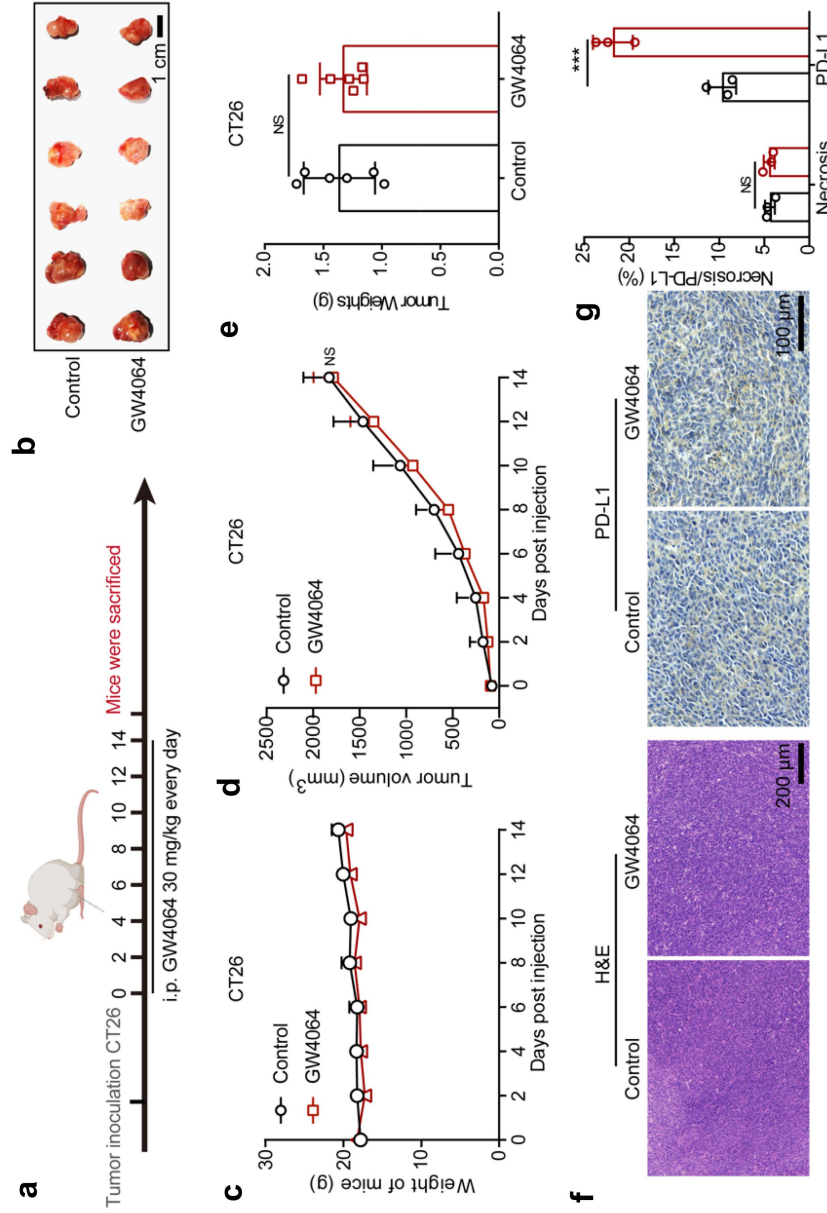


Figure 3. GW4064 did not suppress the growth of CT26 xenograft tumors in vivo. (a) Schematic plan for the administration of GW4064 (30 mg/kg/day) in the CT26 xenograft BALB/c mice model. (b) the tumor photographs, (c) mice weight, (d) tumor growth curves, and the tumor weight (e) in different groups after treatment. Data was presented as mean \pm S.D.; $n = 6$. (f) Representative staining images of HE and PD-L1 in different groups and quantified results (g). Data are shown as mean \pm S.D. ($n = 3$), *** $p < 0.001$.

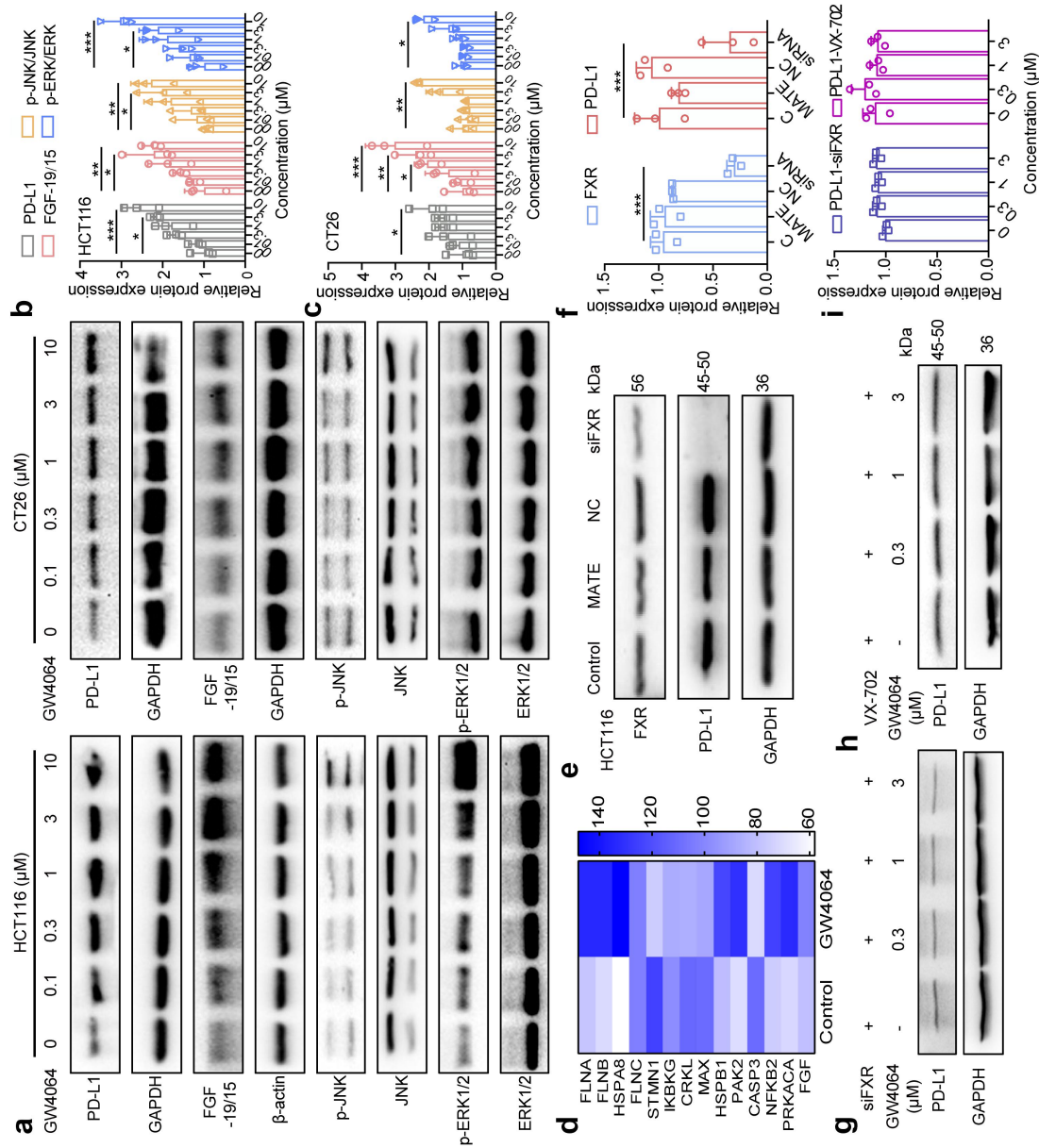


Figure 4. GW4064 upregulated PD-L1 expression in CRC cells through FXR and MAPK signal pathways. (a) the MAPK signal pathway-related proteins JNK and ERK1/2 phosphorylation increased in HCT116 and CT26 cells after treatment with GW4064 for 48 h. Statistical assay of the relative protein contents in HCT116 (b) and CT26 (c) cells. (d) Proteomics results showed that the proteins of MAPK signaling pathway was upregulated after treating with GW4064. (e, f) Knocking down FXR by siRNA, PD-L1 expression was decreased in HCT116 cells. (g-i) Repression of FXR by siRNA and the inhibitor of MAPK signal pathway (VX-702) significantly reversed the upregulatory effect of GW4064 on the expression of PD-L1 in HCT116 cells. Data was presented as mean ± S.D.; n = 3. Statistical significance: *p < 0.05, **p < 0.01, ***p < 0.001.

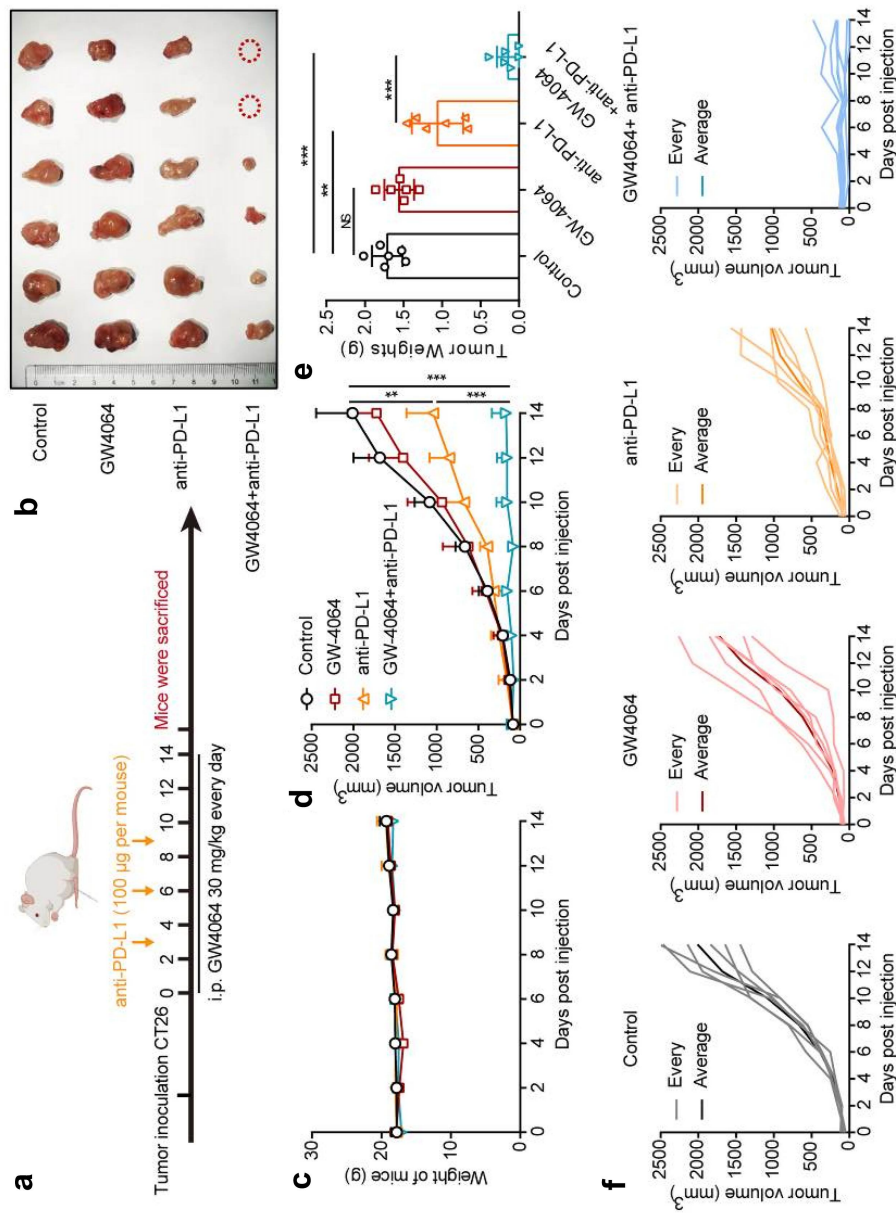


Figure 5. GW4064 enhanced the anti-tumor efficacy of the PD-L1 antibody in vivo. (a) Schematic plan for the administration of GW4064 (30 mg/kg/day) and PD-L1 antibody (100 µg per mouse) in the CT26 xenograft model. The mice weight (c) and tumor volume (d) monitored every two days until day 14, and the tumor weight (e) were, when mice were sacrificed and the resected tumors (b) were photographed. (f) the tumor growth curve of each mouse in each group. Data was presented as mean ± S.D.; n = 6. Statistical significance: *p < 0.05, **p < 0.01, ***p < 0.001.

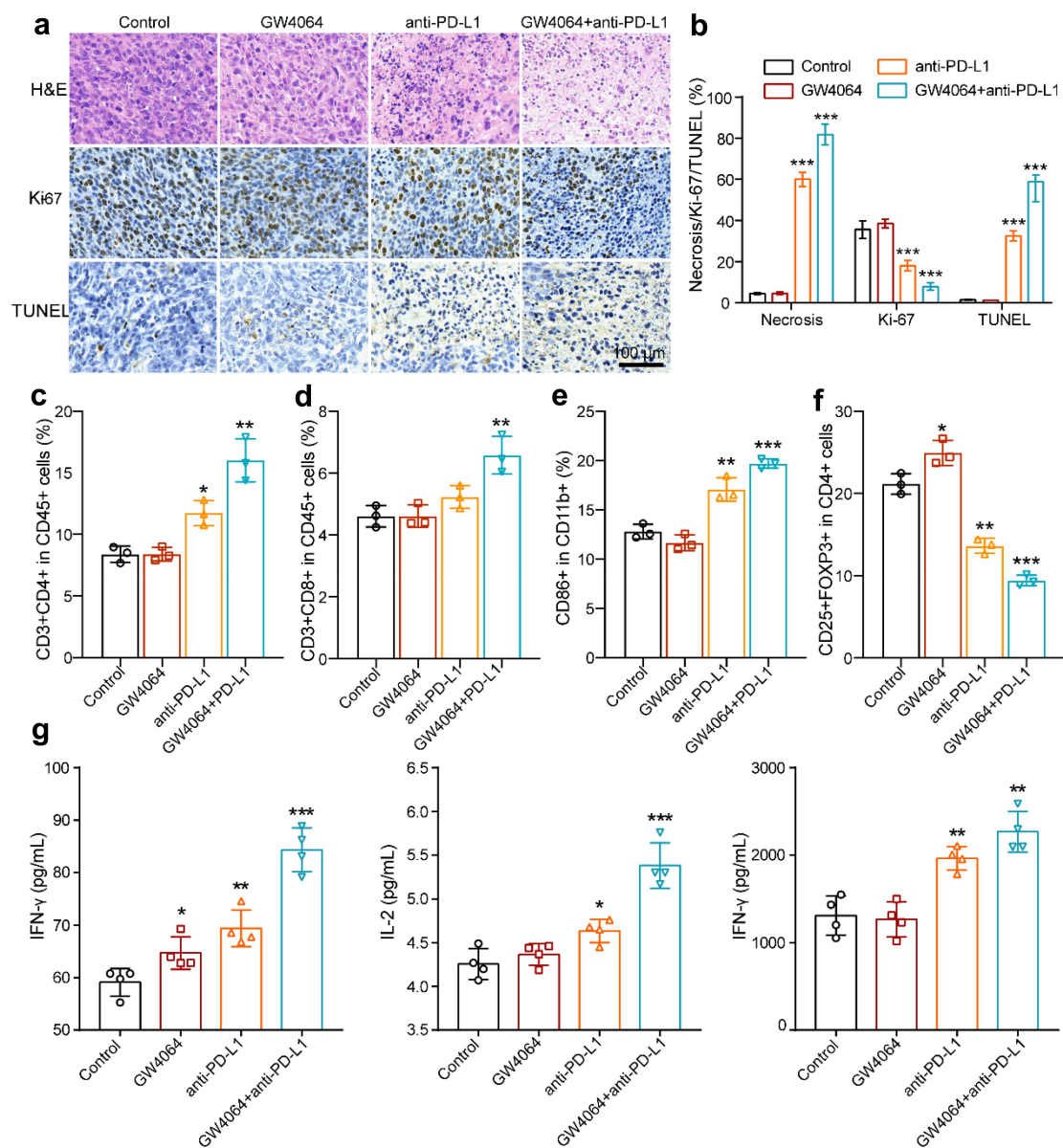


Figure 6. Tumor tissue sections with staining analysis. (a) Representative staining images of HE, Ki-67, and TUNEL in different groups and quantified results (b). (c-d) Percentage of CD4⁺ and CD8⁺ positive cells of tumor tissues in different groups. (e) the proportion of M1 macrophages in tumor tissues in different groups. (f) the proportion of Treg cells in different groups of tumors. Data are shown as mean \pm S.D. (n = 3), ***P < 0.001. (g) the level of IL-2, IFN- γ , and TNF- α in the tumors of different groups. Data are shown as mean \pm S.D. (n = 4), *p < 0.05, **p < 0.01, ***p < 0.001.

weight change and toxic damage in the main organs were observed in these mice (Figure 5C and Fig. S7).

Then, the results of HE, Ki-67, and TUNEL staining confirmed the anti-tumor efficiency of the combination therapy (Figure 6A,B). Furthermore, the recruitment of CD4⁺ and CD8⁺ T cells into tumor sites was evaluated. Moreover, the proportion of M1 macrophages in tumor tissues was significantly increased in the group of GW4064 plus PD-L1 antibody (Figure 6E and Fig. S9A-B). As shown in Figure S6C,D and Fig. S8, the results of flow cytometry showed that the combination therapy of GW4064 and PD-L1 antibody improved CD4⁺ and CD8⁺ T cells infiltration in tumors and decreased Treg cells in tumors (Figure 6F and Fig. S9C-D). The results of Elisa assay showed the increase of IL-2, IFN- γ , and TNF- α in the tumors

after combination therapy (Figure S6G). All these results indicate that GW4064 could enhance the anti-tumor effect of PD-L1 antibody.

Discussion

FXR, known as bile acid receptor, regulates bile acid metabolism mainly in the liver and intestine¹⁰, but also participates in the metabolic balance of glucose, lipids, and amino acids^{11,12}. Emergence evidence suggests that the abnormal expression of FXR is associated with tumorigenesis¹⁹⁻²¹. It is reported that the deficiency of FXR in mice increases colon cell proliferation and spontaneous liver tumors^{38,39}. And the expression of FXR in CRC is lower than that in normal intestinal tissue and is

associated with poor prognosis in CRC patients^{24,25}. Restoring or reactivating the expression of FXR could inhibit the exacerbation and adverse invasion of CRC^{27,28}.

On the contrary, FXR is recognized as a proto-oncogene in NSCLC, and its overexpression is associated with a poor prognosis¹⁶. Interestingly, You et al. found that the immunosuppressive microenvironment caused by overexpression of FXR sensitized NSCLC of FXR^{high}PD-L1^{low} phenotype to anti-PD-1 immunotherapy, thereby enhancing the immunotherapy effect of NSCLC²³. In a subsequent retrospective study, the researchers found that high FXR expression was associated with a higher objective response rate, as well as longer progression-free survival, and overall survival in patients with PD-L1 low expression²². And the CD8⁺ T cells infiltration of tumor tissue had reduced in the NSCLC tumor microenvironment with high expression of FXR²². These suggest that FXR is not only involved in the regulation of tumorigenesis and development, but also in the regulation of immune responses.

With the continuous development of the field of tumor immunotherapy, improving the tumor immune microenvironment, transforming “cold” tumors to “hot” tumors, and combining immune checkpoint inhibitors with chemotherapy and radiotherapy provide novel strategies for cancer treatment^{40,41}. At the same time, ICD has attracted attention due to the activation of anti-tumor-specific immune effects⁴². The mainly specific chemotherapy drugs (such as doxorubicin, oxaliplatin), or the intervention of oncolytic virus, photodynamic therapy, radiation therapy, and other treatments could lead to the release of damage-related molecular patterns, such as HMGB1, CRT, ATP, and other immune signals to initiate systemic anti-tumor immune responses⁴³.

GW4064 is a synthetic nonsteroidal FXR agonist, which has displayed certain anti-tumor effects, and could increase the sensitivity of CRC to chemotherapy drug oxaliplatin^{30,32,44}. In this study, we found that GW4064 could induce cell apoptosis, block cell cycle, and mediate ICD of CRC cells *in vitro*. Disappointingly, GW4064 could not suppress the growth of CT26 xenograft tumors *in vivo*. Considering the important role of PD-L1 in immune response, the expression of PD-L1 after treatment with GW4064 was detected by immunohistochemical assay. We found that the PD-L1 was upregulated significantly after treating with GW4064, which might be the reason of the poor therapeutic efficacy of GW4064 in CT26 tumor-bearing mice.

Then, a proteomic analysis of HCT116 cell treated with GW4064 was performed to explore the mechanisms involved in the upregulation of PD-L1. The results exhibited that GW4064 could upregulate PD-L1 expression in CRC cells via activating FXR and MAPK signaling pathways. Furthermore, we focused on the combination therapy of GW4064 with the immune checkpoint inhibitor PD-L1 antibody for CRC. As expected, the combination of PD-L1 antibody with GW4064 exhibited excellent anti-tumor effects in CT26 xenograft models and increased CD8⁺ T cells infiltration, with 33% tumor bearing mice cured.

Overall, our data illustrate the potential mechanisms of GW4064 to upregulated PD-L1 expression in CRC cells and provide important data to support the combination therapy of PD-L1 immune checkpoint blockade with FXR agonist for CRC patients.

Authors' contributions

Material preparation and data collection were performed by Lu Lu, Yi-Xin Jiang, and Xiao-Xia Liu. Wen-Jie Gu and Jin-Mei Jin analyzed the data. The first draft of the manuscript was written by Lu Lu, Yi-Xin Jiang, Xiao-Xia Liu, and Jin-Mei Jin. Xin Luan, Li-Jun Zhang, and Ying-Yun Guan designed the experiments and revised this manuscript. All authors read and approved the final manuscript.

Disclosure statement

No potential conflict of interest was reported by the authors.

Funding

This work was supported by the National Natural Science Foundation of China (No. 82104194, 82173846, and 82274153), Young Talent Lifting Project of China Association of Chinese Medicine [No. CACM-(2021-QNRC2-A08)], Shanghai Rising-Star Program (No. 22QA1409100), 2021 Shanghai Science and Technology Innovation Action Plan (No. 21S11902800), Three-year Action Plan for Shanghai TCM Development and Inheritance Program [ZY(2021-2023)-0401], and Innovation Team and Talents Cultivation Program of National Administration of Traditional Chinese Medicine (No. ZYYCXTD-D-202004).

Data availability

The authors confirm that the data supporting the findings of this study are available within the article and its supplementary materials.

Ethics approval

All animal experiments were obtained by the ethics committee approval of Shanghai University of Traditional Chinese Medicine.

References

1. Biller LH, Schrag D. Diagnosis and treatment of metastatic colorectal cancer: a review. *JAMA*. 2021;325(7):669–685. doi:10.1001/jama.2021.0106.
2. Mármol I, Sánchez-de-Diego C, Pradilla Dieste A, Cerrada E, Rodríguez Yoldi MJ. Colorectal carcinoma: a general overview and future perspectives in colorectal cancer. *Int J Mol Sci*. 2017;18:18.
3. Fan A, Wang B, Wang X, Nie Y, Fan D, Zhao X, Lu Y. Immunotherapy in colorectal cancer: current achievements and future perspective. *Int J Biol Sci*. 2021;17:3837–3849.
4. Pardoll DM. The blockade of immune checkpoints in cancer immunotherapy. *Nat Rev Cancer*. 2012;12:252–264.
5. Tang Q, Chen Y, Li X, Long S, Shi Y, Yu Y, Wu W, Han L, Wang S. The role of PD-1/PD-L1 and application of immune-checkpoint inhibitors in human cancers. *Front Immunol*. 2022;13:964442. doi:10.3389/fimmu.2022.964442.
6. Wu X, Gu Z, Chen Y, Chen B, Chen W, Weng L, Liu X. Application of PD-1 blockade in cancer immunotherapy. *Comput Struct Biotechnol J*. 2019;17:661–674.
7. Yi M, Zheng X, Niu M, Zhu S, Ge H, Wu K. Combination strategies with PD-1/PD-L1 blockade: current advances and future directions. *Mol Cancer*. 2022;21(1):28. doi:10.1186/s12943-021-01489-2.
8. Franke AJ, Skelton WP, Starr JS, Parekh H, Lee JJ, Overman MJ, Allegra C, George TJ. Immunotherapy for colorectal cancer: a review of current and novel therapeutic approaches. *J Natl Cancer Inst*. 2019;111:1131–1141.
9. Wang Y-D, Chen W-D, Moore DD, Huang W. FXR: a metabolic regulator and cell protector. *Cell Res*. 2008;18:1087–1095.

10. Zhang Y, Kast-Woelbern HR, Edwards PA. Natural structural variants of the nuclear receptor farnesoid X receptor affect transcriptional activation. *J Biol Chem.* 2003;278:104–110.
11. Massafra V, Milona A, Vos HR, Ramos RJJ, Gerrits J, Willemsen ECL, Ramos Pittol JM, Ijssennagger N, Houweling M, Prinsen HCMT. Farnesoid X receptor activation promotes hepatic amino acid catabolism and ammonium clearance in mice. *Gastroenterology.* 2017;152(6):152. doi:10.1053/j.gastro.2017.01.014.
12. Peng X, Wu W, Zhu B, Sun Z, Ji L, Ruan Y, Zhou M, Zhou L, Gu J. Activation of farnesoid X receptor induces RECK expression in mouse liver. *Biochem Biophys Res Commun.* 2014;443:211–216.
13. Li M, Zhang X, Lu Y, Meng S, Quan H, Hou P, Tong P, Chai D, Gao X, Zheng J. The nuclear translocation of transketolase inhibits the farnesoid receptor expression by promoting the binding of HDAC3 to FXR promoter in hepatocellular carcinoma cell lines. *Cell Death Disease.* 2020;11:31.
14. Dai J, Wang H, Shi Y, Dong Y, Zhang Y, Wang J. Impact of bile acids on the growth of human cholangiocarcinoma via FXR. *J Hematol Oncol.* 2011;4:41.
15. De Gottardi A, Touri F, Maurer CA, Perez A, Maurhofer O, Ventre G, Bentzen CL, Niesor EJ, Dufour J-F. The bile acid nuclear receptor FXR and the bile acid binding protein IBABP are differently expressed in colon cancer. *Dig Dis Sci.* 2004;49(6):982–989. doi:10.1023/B:DDAS.0000034558.78747.98.
16. You W, Chen B, Liu X, Xue S, Qin H, Jiang H. Farnesoid X receptor, a novel proto-oncogene in non-small cell lung cancer, promotes tumor growth via directly transactivating CCND1. *Cell.* 2017;7(1):591. doi:10.1038/s41598-017-00698-4.
17. Lee JY, Lee KT, Lee JK, Lee KH, Jang KT, Heo JS, Choi SH, Kim Y, Rhee JC. Farnesoid X receptor, overexpressed in pancreatic cancer with lymph node metastasis promotes cell migration and invasion. *Br J Cancer.* 2011;104(6):1027–1037.
18. Giaginis C, Tsoukalas N, Alexandrou P, Tsourouflis G, Dana E, Delladetsima I, Patsouris E, Theocharis S. Clinical significance of farnesoid X receptor expression in thyroid neoplasia. *Future Oncol.* 2017;13:1785–1792.
19. Torres J, Bao X, Iuga AC, Chen A, Harpaz N, Ullman T, Cohen BL, Pineton de Chambrun G, Ascitti S, Odin JA. Farnesoid X receptor expression is decreased in colonic mucosa of patients with primary sclerosing cholangitis and colitis-associated neoplasia. *Inflamm Bowel Dis.* 2013;19(2):275–282.
20. Liu Y, Chen K, Li F, Gu Z, Liu Q, He L, Shao T, Song Q, Zhu F, Zhang L. Probiotic lactobacillus rhamnosus GG prevents liver fibrosis through inhibiting hepatic bile acid synthesis and enhancing bile acid excretion in mice. *Hepatology (Baltimore, Md).* 2020;71(6):2050–2066. doi:10.1002/hep.30975.
21. Anderson KM, Gayer CP. The pathophysiology of Farnesoid X receptor (FXR) in the GI tract: inflammation, barrier function and innate immunity. *Cells.* 2021;10:10.
22. Wang L, Xu X, Shang B, Sun J, Liang B, Wang X, You W, Jiang S. High farnesoid X receptor expression predicts favorable clinical outcomes in PDL1(low/negative) nonsmall cell lung cancer patients receiving anti-Pd1based chemoimmunotherapy. *Int J Oncol.* 2022;60:60.
23. You W, Li L, Sun D, Liu X, Xia Z, Xue S, Chen B, Qin H, Ai J, Jiang H. Farnesoid X receptor constructs an immunosuppressive microenvironment and sensitizes FXRPD-L1 NSCLC to anti-PD-1 immunotherapy. *Cancer Immunol Res.* 2019;7:990–1000.
24. Lax S, Schauer G, Prein K, Kapitan M, Silbert D, Berghold A, Berger A, Trauner M. Expression of the nuclear bile acid receptor/farnesoid X receptor is reduced in human colon carcinoma compared to nonneoplastic mucosa independent from site and may be associated with adverse prognosis. *Int J Cancer.* 2012;130:2232–2239.
25. Yu J, Li S, Guo J, Xu Z, Zheng J, Sun X. Farnesoid X receptor antagonizes Wnt/ β -catenin signaling in colorectal tumorigenesis. *Cell Death Disease.* 2020;11:640.
26. Guo S, Peng Y, Lou Y, Cao L, Liu J, Lin N, Cai S, Kang Y, Zeng S, Yu L. Downregulation of the farnesoid X receptor promotes colorectal tumorigenesis by facilitating enterotoxigenic bacteroides fragilis colonization. *Pharmacol Res.* 2022;177:106101.
27. Yu J, Yang K, Zheng J, Zhao P, Xia J, Sun X, Zhao W. Activation of FXR and inhibition of EZH2 synergistically inhibit colorectal cancer through cooperatively accelerating FXR nuclear location and upregulating CDX2 expression. *Cell Death & Disease.* 2022;13:388.
28. Li S, Xu Z, Guo J, Zheng J, Sun X, Yu J. Farnesoid X receptor activation induces antitumor activity in colorectal cancer by suppressing JAK2/STAT3 signalling via transactivation of SOCS3 gene. *J Cell Mol Med.* 2020;24:14549–14560.
29. Gong Y, Li K, Qin Y, Zeng K, Liu J, Huang S, Chen Y, Yu H, Liu W, Ye L. Norcholic acid promotes tumor progression and immune escape by regulating Farnesoid X receptor in hepatocellular carcinoma. *Front Oncol.* 2021;11:711448.
30. Hotta M, Sakatani T, Ishino K, Wada R, Kudo M, Yokoyama Y, Yamada T, Yoshida H, Naito Z. Farnesoid X receptor induces cell death and sensitizes to TRAIL-induced inhibition of growth in colorectal cancer cells through the up-regulation of death receptor 5. *Biochem Biophys Res Commun.* 2019;519:824–831.
31. Barone I, Viricillo V, Giordano C, Gelsomino L, Gyorffy B, Tarallo R, Rinaldi A, Bruno G, Caruso A, Romeo F. Activation of farnesoid X receptor impairs the tumor-promoting function of breast cancer-associated fibroblasts. *Cancer Lett.* 2018;437:89–99.
32. Guo J, Zheng J, Mu M, Chen Z, Xu Z, Zhao C, Yang K, Qin X, Sun X, Yu J. GW4064 enhances the chemosensitivity of colorectal cancer to oxaliplatin by inducing pyroptosis. *Biochem Biophys Res Commun.* 2021;548:60–66.
33. Wiśniewski JR, Zougman A, Nagaraj N, Mann M. Universal sample preparation method for proteome analysis. *Nat Methods.* 2009;6:359–362.
34. Forman BM, Goode E, Chen J, Oro AE, Bradley DJ, Perlmann T, Noonan DJ, Burka LT, McMorris T, Lamph WW. Identification of a nuclear receptor that is activated by farnesol metabolites. *Cell.* 1995;81:687–693.
35. Joo JH, Jetten AM. Molecular mechanisms involved in farnesol-induced apoptosis. *Cancer Lett.* 2010;287:123–135.
36. Joo JH, Liao G, Collins JB, Grissom SF, Jetten AM. Farnesol-induced apoptosis in human lung carcinoma cells is coupled to the endoplasmic reticulum stress response. *Cancer Res.* 2007;67:7929–7936.
37. King AP, Wilson JJ. Endoplasmic reticulum stress: an arising target for metal-based anticancer agents. *Chem Soc Rev.* 2020;49:8113–8136.
38. Yang F, Huang X, Yi T, Yen Y, Moore DD, Huang W. Spontaneous development of liver tumors in the absence of the bile acid receptor farnesoid X receptor. *Cancer Res.* 2007;67:863–867.
39. Maran RR, Thomas A, Roth M, Sheng Z, Esterly N, Pinson D, Gao X, Zhang Y, Ganapathy V, Gonzalez FJ. Farnesoid X receptor deficiency in mice leads to increased intestinal epithelial cell proliferation and tumor development. *Cell.* 2009;328:469–477.
40. Bader JE, Voss K, Rathmell JC. Targeting metabolism to improve the tumor microenvironment for cancer immunotherapy. *Mol Cell.* 2020;78:1019–1033.
41. Galon J, Bruni D. Approaches to treat immune hot, altered and cold tumours with combination immunotherapies. *Nat Rev Drug Discov.* 2019;18:197–218.
42. Kroemer G, Galluzzi L, Kepp O, Zitvogel L. Immunogenic cell death in cancer therapy. *Annu Rev Immunol.* 2013;31:51–72.
43. Kroemer G, Galassi C, Zitvogel L, Galluzzi L. Immunogenic cell stress and death. *Nat Immunol.* 2022;23:487–500.
44. Alawad AS, Levy C. FXR agonists: from bench to bedside, a guide for clinicians. *Dig Dis Sci.* 2016;61:3395–3404.